Universal Journal of Computational Analysis **2 (2014), 27-45**
www.papersciences.com

Void Shape Evolution of Silicon Simulation: Non-linear Three-dimensional Curvature Calculation by First Order Analysis

C. Grau Turuelo, B. Bergmann, C. Breitkopf
Technical University Dresden, Faculty of Mechanical Engineering
Institute of Power Engineering, Chair of Technical Thermodynamics
01062 Dresden, Germany
Constantino.Grau@mailbox.tu-dresden.de

Abstract
Simulations of SON structures were carried out by the use of FEM and the arbitrary Lagrangian-Eularian (ALE) method through the software COMSOL Multiphysics®. A novel time-dependent *"virtual"* curvature algorithm based on non-linear surface diffusion kinetics for FEM simulations is presented. The model describes the evolution from a cylindrical trench etched on silicon to an equilibrium sphere by thermal annealing. An initial aspect ratio (length/diameter) of 2.22-6.66 is determined for creating an ESS. For more than one ESS, the aspect ratio limits are also investigated. With this model, at equilibrium, the step size increases with the length of the initial trench once it is closed while the SON layer increases with the initial cylindrical depth. The temperature enhances the velocity of the evolution.

Key Word and Phrases
Silicon-On-Nothing (SON), Empty-Space-In-Silicon (ESS), Void Shape Evolution, Surface Diffusion, Kinetic Modelling, Chemical Potential, Micro-Structures, Annealing, Deoxidizing Ambient, Finite Elements Method (FEM), Simulation, Comsol, Curvature Driven Phenomena, First Order Analysis, Surface Instabilities

1. Introduction

SON (Silicon-on-nothing) devices have progressively gained prominence in the research field during the last years due to its possibility of implementation in different semiconductor applications at a reduced cost. A SON structure consists of the formation of an empty space in silicon (ESS), or silicon-void-silicon, through different manufacturing methods. Depending on the application, the empty space can be differently treated. Among those applications, the one with the highest interest is the employment of the silicon-nothing-silicon structure as the base for building transistors (Fig. 1a) (the empty space serves as an insulator to prevent electronic migration from the device to the substrate) and other semiconductor devices while having similar current SOI (Silicon-on-insulator) performance.

Regarding the characteristics and electric performance of SON devices, several studies indicate similar threshold voltages and operational currents for SON and SOI devices which improves its interchangeability [1]. However, while the on/off transitions in SON devices can be about 30-40% faster than bulk devices [1]-[4], SOI devices can provide an additional 10-20% of speed increase [1]. SON devices also show some advantages over SOI ones like the ability of making low voltage devices because of its potential for manufacturing thinner channels [1-4] or a better heat tolerance due to the lower parasitic capacitance/resistance and reduced insulator area [2], [3]. Nevertheless, if the SOI layer has the same dimensions of a SON one, then, SON presents a higher thermal resistance of about 37% [5].

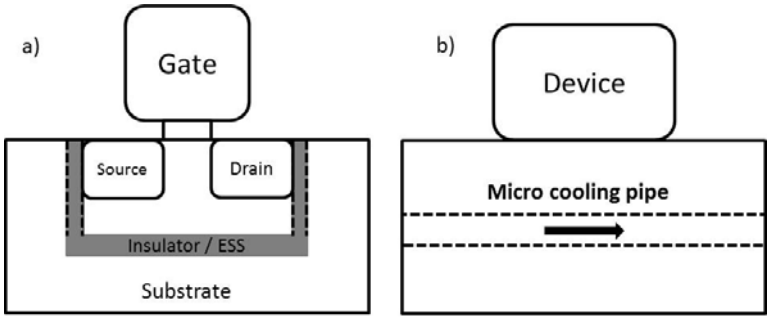

Fig. 1 Basic scheme of two SON applications: a) SON transistor; b) micro cooling.

On the other hand, having a hole below the main electronic structure presents mechanical disadvantages such as bending and appearance of small cracks. In order to overcome this, another way for imitating standard SOI devices through the presented SON technology, without mechanical disadvantages, is to fill the empty space between the two silicon layers with an insulator (for instance, silicon oxide) by etching holes at the sides of the empty-space-in-silicon and fill the space with an oxidizing gas [6]. The result would be similar to that in standard SOI processing with the difference that, in SON fabrication, the insulator can be solely applied in localized zones (usually under the gate and between the drain and source connections of a MOSFET) and not in the whole structure.

Two other important applications are pressure sensors and micro cooling (Fig. 1b) [7]. A pressure sensor can be built using the pressure difference between the external gas and the pressure inside the empty-space-in-silicon. This would cause a bending on the upper layer proportional to the pressure difference. By applying a piezoelectric/piezoresistive layer on the top, the external pressure can be measured. Furthermore, the creation of pipe shaped cavities underneath any electronic or electric device can lead to micro channels which can refrigerate the system closer to the heating source, improving its effectiveness. For this last application, the void shape evolution, as explained in the following lines, is particularly suitable.

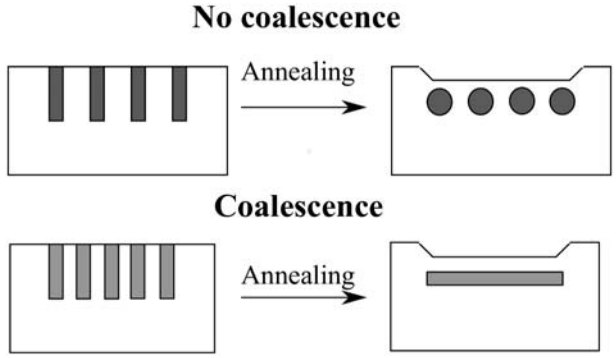

Fig. 2 Scheme of the SON process with and without coalescence.

Several techniques have been developed to create SON morphologies such as lateral etching [2], [3], [8], [9], or double He+/ He+ and H+ ion co-implantation with posterior annealing [10], [11]. Lately, another form for obtaining SON microstructures has been developed: “void shape evolution in silicon” [12]-[15]. It consists of the following subsequent steps: firstly, some trenches are etched in a silicon wafer; secondly, the wafer is exposed to high temperatures (about 1100 °C) and medium vacuum conditions (about 10 Torr) annealing under a deoxidizing atmosphere such as hydrogen. The sum of these factors enhances the surface diffusion on the trench surface, provoking a geometry evolution which leads to an empty space in silicon (ESS) with a silicon layer above it

(SON) as shown in Fig. 2. This process is simpler and cheaper than direct etching but the prediction of the final geometry as well as the control of the process is still under discussion.

Theories were developed to explain the kinetics of this process based on *Mullins' theory* [14], [16]. Those approaches rely on the variation of the surface chemical potential as the driving force for the transport phenomena. The chemical potential of a surface can be defined as the free energy change associated with the transfer of one atom from a reference system (infinite crystal) to the given surface. The addition or removal of atoms of the surface (making it more convex or concave, respectively) modifies its shape which is characterized by the curvature. The curvature represents the continuous change of orientation of the surface so that its variation indicates which points are more favorable to gain or lose atoms from or to the neighboring surfaces, respectively. By the utilization of the *Nernst-Einstein* relation and the theory behind the surface diffusion, a relation between the normal velocity of the surface and the variation of its curvature is found through the definition of a driving force due to the mentioned chemical potential. Thus, the equation of the evolution by a surface diffusion mechanism has a solid and demonstrated base. However, the result of this theory is a non-linear PDE (Partial Differential Equation) that presents a high dependence on the evolving geometry and makes the prediction and simulation of these evolving morphologies a complicated task to solve.

Once the theory is determined, the next step is to select the simulation method and how it will be simulated, that is to say, algorithms and solvers. Concerning the method choice, the characteristic values reported by the literature are in the scale of micrometers and hundreds of seconds. For this scale, a continuum method is suitable [17]. The most representative computational method for continuum models is FEM (Finite Element Method) which will be used for the simulation of this specific surface diffusion model.

Regarding the solution algorithm, the method which is mainly used for surface energy minimization or surface tension related problems is the Level-Set or the Phase Field method [18]-[20]. These two methods are commonly used for Fluid Mechanics coupled with the Navier-Stokes equation. The drawback of this method is that it is intended to be a volumetric method for volumetric phenomena. In the case of Fluid Mechanics, the definition of the fluid particle is employed and thus the variables are expressed in the corresponding unit per volume. However, the phenomenon that is described in this work is a surface one so that a volumetric approach is difficult to define. Furthermore, the equation which drives the surface diffusion would need a fourth order non-linear PDE (Partial Differential Equation) of the phase field variable which is stiff and difficult to solve, especially, at high geometry orders [21]-[23]. There have been some approaches with this method but the computation time was so high that only small variations could be accurately simulated. In addition, it needs a relative small mesh to have a stable solution and its numerical stabilization (addition of a compression and a viscosity for layer stability) depends on parameters which must be chosen carefully in every simulation as it can lead to a large diffusive effect or a big volume enlargement or reduction [24], [25].

The aim of this work is to overcome this modeling challenge and compare the simulation results with previous literature data. For this purpose, a surface method that can reproduce the velocity of the surface by the direct application of the non-linear surface diffusion equations was chosen: the arbitrary Lagrangian-Eulerian (ALE) method [26]. The drawback of this method is the lack of precision when computing the divergence of the normal as the mesh size is required to be comparable to the expected displacement which, in this case, corresponds to the initial hollow size. As a consequence, it leads to a very poor calculation of the curvature. This problem is addressed in this work by defining a "*virtual"* curvature function which is based on the extraction of specific SON thermodynamic kinetic properties. Finally, the simulations are made in COMSOL Multiphysics® for a three dimensional system to get their representative values so as to understand and control the process. These obtained values are compared with those of previous literature work.

2. Theoretical Kinetic Model

The theoretical kinetic model presented in this paper is a simplified approach for the calculation of the velocity of the morphological evolution of microstructures driven by surface diffusion. It is

based on the minimization of surface energy which, at the same time, acts as the driving force of the mentioned surface diffusion phenomenon. The surface area of an arbitrary body depends on its shape. The characterization of that shape is given by the curvature of the surface as it will be evidenced below. Thus, the change of curvature will provoke a change in the velocity and, consequently, the evolution of the empty space in silicon.

2.1 Chemical Potential and Free Energy Minimization

The "void shape evolution" process is driven by changes of the free energy on a given surface. The overall free energy, G, of a surface can be described as:

$$G = \gamma S \tag{2.1}$$

where γ is the surface energy density (J/m^2) and S is the surface area (m^2).

When the shape of the surface is modified, the amount of free energy stored on that surface changes. The thermodynamic variable which describes this variation is the chemical potential (μ):

$$\mu = \delta G \tag{2.2}$$

The chemical potential is defined as the free energy change associated with the transfer of one atom from a reference system (infinite crystal) to an arbitrary surface. Making a geometrical analysis when a surface gains an atom with an isotropic surface energy density [16], [27], it can be demonstrated that the chemical potential is directly dependent on the curvature as follows (neither external stresses nor electric fields):

$$\mu = \Omega\gamma(K_1 + K_2) = \Omega\gamma K \tag{2.3}$$

where Ω is the atomic volume (m^3/atom), K_1 and K_2 are the two main curvatures (1/m) of the surface. The curvature reflects the continuous change of an arbitrary surface and it is used for determining the area of closed curved body. The term full curvature (K) is used, from this point, as the sum of the two main curvatures.

For instance, the chemical potential of a cylinder (R_C) and a sphere (R_S), respectively, is:

$$\mu_C = \Omega\gamma\left(\frac{1}{R_C}\right) \tag{2.4}$$

$$\mu_C = \Omega\gamma\left(\frac{2}{R_S}\right) \tag{2.5}$$

where R_C and R_S are the radius of the cylinder and the sphere, respectively. Accordingly, $1/R_C$ and $2/R_S$ are the curvature values for a cylinder and a sphere.

2.2 Three-dimensional Cartesian Kinetics

When a FEM solver such as COMSOL® is used, it is difficult to define local coordinates which could track a moving plane. An exception would be a small deformation of a solid whose initial surface is almost unperturbed during the whole simulation.

The kinetics driven by the non-linear surface diffusion equation, when it was defined by Mullins, is based on a local coordinate system (two parallel and one normal direction) which is suitable for small grooves on a material surface [16]. With such a small deviation of the smoothness of the surface, those local coordinates can be transformed into local angles and its reducing/increasing rate with the time.

In a system where the whole geometry is susceptible to change, global coordinates become necessary as it is not possible to define an angle in every point of the surface. Thus, we developed a model based on "Mullins' theory of thermal grooving" [16], whose equations have been modified in order to be able to build a three-dimensional, cartesian coordinate system for its use in our simulation program (COMSOL® 4.2).

Taking into account only the surface diffusion phenomenon [14]-[16], [27], [28], the driving force caused by the chemical potential can be defined theoretically as:

$$\mathbf{F} = -\nabla\mu = -\Omega\gamma\left(\frac{\partial K}{\partial x}\mathbf{i} + \frac{\partial K}{\partial y}\mathbf{j} + \frac{\partial K}{\partial z}\mathbf{k}\right) \tag{2.6}$$

Using the Nernst-Einstein relation and the Boltzmann distribution [28], the drift velocity of the particles in all directions is:

$$\overline{\mathbf{v}} = -\frac{D_S\Omega\gamma}{k_B T}\nabla K = -\frac{D_S\Omega\gamma}{k_B T}\left(\frac{\partial K}{\partial x}\mathbf{i} + \frac{\partial K}{\partial y}\mathbf{j} + \frac{\partial K}{\partial z}\mathbf{k}\right) \tag{2.7}$$

where D_S is the surface diffusion coefficient (m^2/s), k_B is the Boltzmann constant (J/K) and T is the temperature (K). Multiplying the particle's velocity by the surface atomic density, X_S (atom/m^2), an expression for the atomic current in every direction is yielded:

$$\mathbf{j} = -\frac{D_S X_S\Omega\gamma}{k_B T}\nabla K = -\frac{D_S X_S\Omega\gamma}{k_B T}\left(\frac{\partial K}{\partial x}\mathbf{i} + \frac{\partial K}{\partial y}\mathbf{j} + \frac{\partial K}{\partial z}\mathbf{k}\right) \tag{2.8}$$

Now, consider a small element of the surface of the body. Let v_n be the velocity of the solid surface. That velocity is normal to the solid surface and it generates a scalar field on that solid surface. It can be observed that v_n/Ω is the number of atoms gained per unit area and per unit time. The divergence of the current of atoms is the number of atoms diffusing out of the surface per unit area and per unit time. If this is the only phenomenon, the final non-linear kinetic equation driven by surface diffusion results from the equality of the two given definitions:

$$v_n = \frac{D_S X_S\Omega^2\gamma}{k_B T}\Delta K = \frac{D_S X_S\Omega^2\gamma}{k_B T}\left(\frac{\partial^2 K}{\partial x^2} + \frac{\partial^2 K}{\partial y^2} + \frac{\partial^2 K}{\partial z^2}\right) \tag{2.9}$$

Finally, the velocity evolution, **v**, of the surface is just the product of the normal velocity and the corresponding normal vector, **n**, at every point:

$$\mathbf{v} = v_n\mathbf{n} \tag{2.10}$$

This equation defines the kinetics of the process on every point of the surface depending on the curvature which is the base of all the calculations.

It is important to notice that the divergence defined here is the divergence related to the surface and not to the volume because the curvature is a surface phenomenon. In some bibliography, this divergence can be found with the subscript "s" [16], [21], [23].

2.3 Geometrical Evolution Analysis

The "void shape evolution" is a time-dependent process. In order to simplify the solution of the non-linear equation (2.9), this time dependence must be yielded from an analytical equation. This equation must give a view of the evolution from a cylindrical trench to a spherical empty space in silicon. For such a geometrical change, a sinusoidal perturbation on the surface is taken as the mechanism which will drive the evolution at a characteristic wavelength, λ [12], [27]. The development of this evolution analysis is based on Rayleigh's instabilities [29]. For this approach, it is assumed that:

1) There is a perturbation on the surface of the initial cylinder caused by the formation of vacancies at high temperatures.
2) The perturbation will be propagated along the trench depth (vertical) direction.
3) The perturbation has a wave form and each wavelength (λ) creates an entire geometry change to a final sphere by the non-linear diffusion equations that are used in the model.
4) The void volume remains constant during the full process (volume preservation).
5) The "void shape evolution" process is driven by a decrease of the surface free energy.

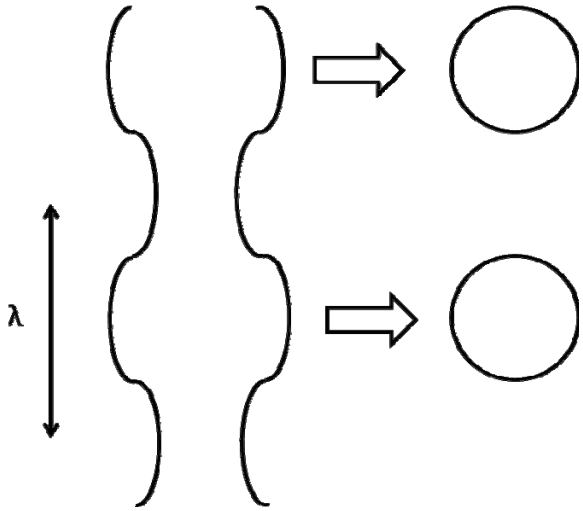

Fig. 3 Scheme of the void shape evolution from a perturbed cylinder.

When analyzing the geometry evolution from a cylinder of length λ to a sphere with a lower surface free energy (fifth assumption, Fig. 3) [30], a condition, which must be fulfilled for an energetically allowed process, is achieved:

$$\lambda > \frac{9R_{\mathrm{C}}}{2} \tag{2.11}$$

After that, one can thus use cylindrical coordinates on the given initial cylindrical geometry (center of coordinates at the bottom of the depth and at the center of the circle) and define the perturbed radius, using a waveform function [27], as (assuming volume preservation):

$$r = R_{\mathrm{C}}\left[1 - \frac{\varepsilon(t)^2}{4} + \varepsilon(t)\cos(kz)\right] \tag{2.12}$$

where ε is the amplitude of the perturbation ($\varepsilon << 1$ in the beginning), z is the cylindrical coordinate in the vertical direction and k is $2\pi/\lambda$ which is the function that drives the oscillation depending on the wavelength λ.

Equation (2.12) is a non-linear equation. For this specific perturbation analysis, it is necessary to linearize the equation around the variable ε in order to make a first order analysis and prevent further non-linearity issues:

$$r = R_{\mathrm{C}}\left[1 + \varepsilon(t)\cos(kz)\right] \tag{2.13}$$

The two main curvatures (negative sign reference for a concave surface) can be calculated for the r direction (the inverse of the cylindrical radius) and z direction (second derivative with respect to the z direction), respectively, as:

$$K_1 = -\frac{1}{r} = -\frac{1}{R_{\mathrm{C}}\left[1+\varepsilon(t)\cos(kz)\right]} \approx -\frac{1}{R_{\mathrm{C}}}\left[1-\varepsilon(t)\cos(kz)\right] \tag{2.14}$$

$$K_2 = \frac{\partial^2 r}{\partial z^2} = -R_{\mathrm{C}}\varepsilon(t)k^2\cos(kz) \tag{2.15}$$

At the same time, the normal velocity of the surface can be approximately calculated as:

$$\frac{\partial r}{\partial t} = R_{\mathrm{C}}\frac{\mathrm{d}\varepsilon}{\mathrm{d}t}\cos(kz) \tag{2.16}$$

Making the equality of (2.9) with the velocity given by (2.16):

$$\frac{\mathrm{d}\varepsilon}{\mathrm{d}t} = \frac{\varepsilon}{\tau} \tag{2.17}$$

where:

$$\tau = \frac{R_C^4 / B}{(kR_C)^2 - (kR_C)^4} \tag{2.18}$$

$$B = \frac{D_S X_S \Omega^2 \gamma}{k_B T} \tag{2.19}$$

$$k = \frac{2\pi}{\lambda} \tag{2.20}$$

being τ the growth constant. ε can be calculated, setting ε (0) as the initial value, from (2.17):

$$\varepsilon(t) = \varepsilon(0) \exp\left(\frac{t}{\tau}\right) \tag{2.21}$$

The "void shape evolution" can be driven by sinusoidal perturbations whose wavelength fulfills the condition (2.11) and provokes a positive growth constant τ ($\lambda > 2\pi R_C$ from (2.18)). The predominant wavelength will be the one which makes the fastest evolution. Consequently, the value of λ must be the one that makes the highest perturbation in the beginning (t ≈0). In order to do that, ε(t) must be forced to be as big as possible, that is to say, making τ as small as possible.

That minimum can be found by calculating the first derivative of τ:

$$\frac{d\tau}{d\lambda} = 0 \Rightarrow \lambda_C = \sqrt{2}\,2\pi R_C \approx 8.89 R_C \tag{2.22}$$

In addition, to prove that this is a minimum, the second derivative of τ when $\lambda = \lambda_C$ is calculated:

$$\frac{d^2\tau}{d\lambda^2}(\lambda_C) = \frac{4R_C^2}{\pi^2 B} \Rightarrow \lambda = \lambda_C \rightarrow \text{minimum} \tag{2.23}$$

This result provides a characteristic wavelength for the "void shape evolution" process from a geometrical analysis that relies on an initial perturbation which governs the full surface development. Using this value in the geometrical evolution, the spherical radius, R_S, can be calculated as (by volume preservation):

$$R_S = 1.88 R_C \tag{2.24}$$

3. Curvature Calculation

The curvature is an indicator of how the surface orientation changes. Every surface can be characterized by its normal at every point. Thus, the spatial variance of the mentioned normal results in the calculation of the surface curvature [31]:

$$K = \nabla \mathbf{n} \tag{3.1}$$

For solving equation (3.1), the arbitrary Lagrangian-Eulerian method (ALE) was initially employed through the software COMSOL Multiphysics®. It was observed that this operation is very sensitive to adjustments of the mesh element size as hinted out in the introduction. The large displacement of the surface needs a very coarse element size which produces a very poor curvature calculation. In order to overcome this, the right mesh and the proper boundary conditions must be chosen depending on the characteristic values found in section 2 so as to determine a suitable evolution.

First of all, based on the observation of the phenomenon, the following assumptions for those boundary conditions are made:

1) At the beginning of the evolution ($t = 0$), a perturbation on the surface appears, similar to (2.13), which makes a distortion on the cylindrical surface. The reason behind this is a vacancy movement generated by the high temperature.

2) At an infinite time ($t = \infty$), the surface shape will present the equilibrium state which is, in this case, a perfect sphere.

3) The function used must have a "start-stop" feature with the following characteristics:
   a) A fast initial evolution because of the action of the initial perturbation whose growth constant is determined in (2.18).
   b) The velocity of the evolution must decrease when it approaches to the equilibrium shape.
   c) When the equilibrium shape is achieved, the boundary conditions must stop the shape movement.

4) The sinusoidal solution (calculated by the use of (2.14) and (2.15)) must have a wavelength of $\lambda = 8.89R_C$.

For building such a function, a study of the equation of the total curvature, (2.14) and (2.15), must be made:

$$K = -\frac{1}{R_C\left[1+\varepsilon(t)\cos(kz)\right]} - R_C\varepsilon(t)k^2\cos(kz) \tag{3.2}$$

The first term in (3.2) will be dominant in the beginning of the movement while the second term will lead the evolution afterwards. The first term of the equation represents an exponential decay of the curvature until it achieves a certain time. However, the second term will evolve to the infinite so that it will not achieve equilibrium at all if used in this form.

From this point, a time where only the first term will be predominant will be assumed to overcome the instability of the complete non-linear equation, which is provoked mainly from the first order approximation of the radius function [27]. An equation for defining the suitable boundary conditions will be developed based on the first term of equation (3.2) with a small modification to be able to take into account the final equilibrium condition. Firstly, for simplification purposes, instead of using the full sinusoidal function from the equation (3.2), only the peak values of the waveform will be calculated:

$$K_p = C_1\left[1 + C_2\exp\left(-\frac{t}{\tau}\right)\right] \tag{3.3}$$

where K_p represents the peak value of the virtual curvature function which is close to the real value of the curvature; C_1 and C_2 are variables that depend on the z coordinate; t is the time; and τ is the growth constant. This function describes the evolution from a curvature peak value of $C_1[1+C_2]$ at $t = 0$ to an equilibrium value of C_1 at $t = \infty$ through a very fast evolution in the beginning controlled by the growth constant calculated in equation (2.18).

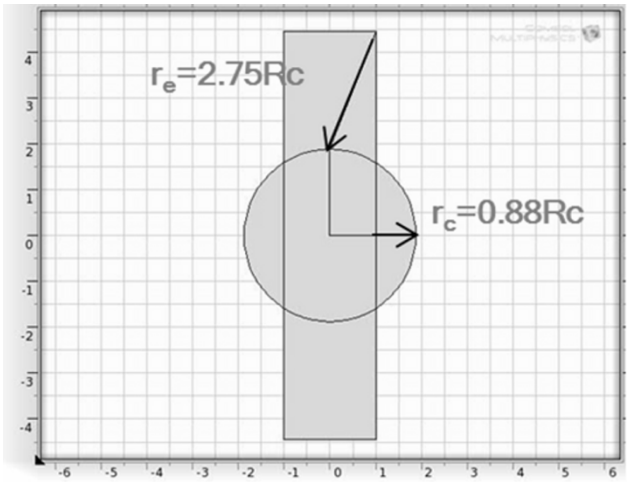

Fig. 4 Movement of the center and extreme points of the waveform (COMSOL®).

The peak values of the waveform for the transformation of a cylinder into a sphere will take place at the center and the extreme sides of a cylinder whose vertical length is λ (Fig. 4). That means that if the bottom of the cylindrical trench is defined as the origin of coordinates and the cylinder length is larger than λ, then, it follows a succession of minimum peak curvature value every $z = n\lambda$ (value of the perturbation at the extreme sides, according to Fig. 4, with the sub index E) and the maximum peak value every $z = (n+1/2)\lambda$ (value of the perturbation at the center, according to Fig. 4, with the sub index C) for $n = 0, 1, 2,\ldots,\infty$. Their definitions are detailed in the subsequent sections.

3.1 Virtual Curvature Calculation for the Central Part of the Waveform ($z = (n+1/2)\,\lambda$)

The peak definition used on these points consists of two separate temporal conditions: (i) the curvature at the beginning of the process ($t = 0$) is equivalent to the curvature of an unperturbed cylinder, $-1/R_C$, which is negative because of (3.1) (normal directed inwards the center of the cylinder); and (ii) the curvature at the end of the process ($t = \infty$) is equivalent to the curvature of the final sphere, $-2/R_S$ or, by the use of (2.24), $-2/1.88R_C$. Writing it into an equation system:

$$\begin{aligned} K_C(t=0) &= -\frac{1}{R_C} \\ K_C(t=\infty) &= -\frac{2}{1.88R_C} \end{aligned} \tag{3.4}$$

which yields from (3.3):

$$K_C = -\frac{2}{1.88Rc}\left[1-0.06\exp\left(-\frac{t}{\tau}\right)\right] \tag{3.5}$$

This temporal boundary condition must be defined on every z (vertical coordinate) of the trench surface that fulfills $z = (n+1/2)\,\lambda$.

3.2 Virtual Curvature Calculation for the Extreme Part of the Waveform ($z = n\lambda$)

The peak definition used on these points should be the same as the ones pointed in the section 3.1. However, it would prevent the evolution of the structure because the sinusoidal wave would transform into a flat line (waveform with no amplitude). In order to avoid this, the initial perturbation must be included in this peak condition.

Firstly, the condition at the final stage ($t = \infty$) will remain the same as in the previous case because the equilibrium results in a spherical shape which will be the stopping point. However, for

obtaining the initial condition, the kinetic equation (2.9) has to be analyzed. As it is known, the initial velocities of different points are proportional to the path that they have followed during a certain time. For the same principle, looking at (2.9), the initial velocities will be determined by the initial curvature values of certain positions so that it can be assumed that $\Delta r \sim K$ on any given point when all other parameters are constant. Using a linear approach as indicated in Fig. 4, it yields:

$$\frac{\Delta r(\text{edge})}{\Delta r(\text{center})} = \frac{r_e}{r_c} \approx \frac{K_E(0)}{K_C(0)} = \frac{2.75}{0.88} \tag{3.6}$$

Equation (3.6) defines the parameters needed for the initial temporal condition:

$$\begin{aligned} K_E(t=0) &= -\frac{2.75}{0.88R_C} \\ K_E(t=\infty) &= -\frac{2}{1.88R_C} \end{aligned} \tag{3.7}$$

which finally yields from (3.3):

$$K_E = -\frac{2}{1.88Rc}\left[1+1.94\exp\left(-\frac{t}{\tau}\right)\right] \tag{3.8}$$

This temporal boundary condition must be defined on every z (vertical coordinate) of the trench surface that fulfills $z = n\lambda$.

3.3 Characteristics and Implementation

The conditions (3.5) and (3.8) must be fulfilled for a correct evolution of the geometry. As a result, a "virtual" curvature function must be created. This analytical function will replace the calculation of the real curvature with a perturbation based virtual curvature which is close to the real one. It can reduce the mesh dependence (a critical factor for the ALE method) and provide faster simulations.

Furthermore, this kind of functions can be used to represent the evolution of phenomena which have similar characteristics to the Rayleigh instabilities (splitting geometries which are curvature driven, for example, due to surface tension) where an analysis similar to that in section 2.3 can be performed. For its use with other geometries and/or phenomena, new growth constants and virtual curvature functions must be found.

The implementation can be done in two ways:

1) By defining a vertical distance between mesh nodes of $\lambda/2$: the first node point is placed at the bottom of the trench and the rest of them follow along the z-direction where the vertical distance between the last two nodes must be equal or lower than $\lambda/2$. On those points, the values of the virtual curvature defined on sections 3.1 and 3.2 must be forced as boundary conditions. (2.10) and (3.1) must be solved on the trench surface where the value of K will give as a result the virtual curvature function.

2) By solving (2.10) and replacing (3.1) directly by this virtual curvature function:

$$K_v = \frac{(K_C + K_E)}{2} - \frac{(K_C - K_E)}{2}\cos\left(\frac{2\pi(z - z_0)}{\lambda}\right) \tag{3.9}$$

where z_0 is the z-coordinate of the bottom of the trench. This second way is more recommended as it is mesh independent. However, the user must be aware of the expected displacement of the geometry as the mesh size must have the same order of magnitude as the expected displacement in the ALE method. Otherwise it could collapse or inverse the geometry. For a better output due to the large mesh elements, at least, a cubic discretization is recommended.

There are several advantages in COMSOL when equation (3.9) is employed. First of all, one PDE (3.1) is not necessary to be calculated. Instead of that, the non-linear function (3.9) is directly applied as a scalar field which also helps with the calculation of the equation (2.9). It is independent on the geometry evolution but dependent on the initial geometry and conditions which are already known before the simulation.

As a consequence, the calculation is highly simplified and the simulation time is reduced, at least, to the half. Moreover, it skips the direct calculation of the normal divergence which, with coarse meshes (obligatory in this problem), is very imprecise and causes inverted elements, resulting in a geometry crash or a lack of convergence. It was the most optimal way to couple this problem with the ALE method in COMSOL.

4 Results and Discussion

In order to carry out the simulations, the parameter "B", see (2.19), needs to be determined. For simplicity, an isotropic crystal orientation will be assumed: <100>. The surface diffusion coefficient (D_S) will be adapted to the expression $0.1\exp(2.3\text{eV}/k_BT)$ m^2/s [32] where k_B is the Boltzmann constant and T is the temperature of the system. X_S is the atomic surface density, for <100>: $1.13\cdot10^{-9}$ mol/cm^2. The atomic volume for silicon (Ω) is 12.06 cm^3/mol.

The surface energy density for <100> is 1.2 J/m^2 [33]. All the previous values must be used in the international system of units. The movement of the geometry was computed by the use of the "Moving Mesh" module, based on ALE, in COMSOL Multiphysics® but it could be implemented in any other FEM solver. The surfaces interpenetrate each other when in contact. The simulation was made on a 3D system, but for a better overview, only 2D sections will be shown.

4.1 Geometry Dependence

In order to observe how the evolution behaves with this model, we used a simulation example whose geometry has an order of magnitude similar to previous experimental results found in the bibliography [12]-[15]. The initial geometry is a cylindrical trench whose length and diameter is shown on the respective picture. Only one trench is simulated as a simplification of real cases due to the coalescence that can occur with the arrangement of trenches in a row as it was shown in Fig. 2.

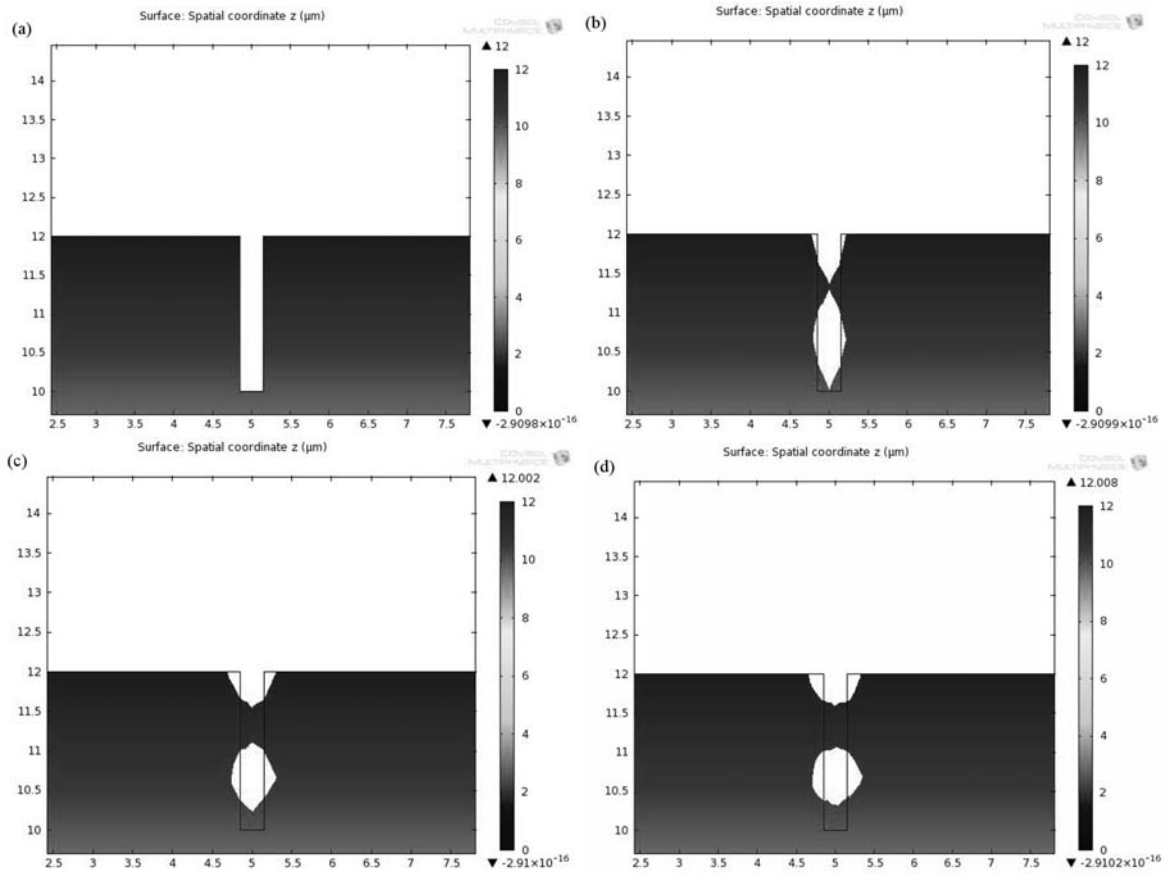

Fig. 5 Shape evolution of a trench with a trench diameter of 0.30 µm, trench length of 2 µm at 1100°C after a) 0 s; b) 10 s; c) 20 s; d) 90 s.

The shape development of Fig. 5 can be described in the following steps:

1) at t = 0s, the initial cylindrical trench is presented,
2) at t = 10s, a "pinch-off" is created on the top of the hole. The "pinch-off", or neck, shows how the empty space in silicon is created as a void shape which is separated from the outer void.
3) From t = 20s, an ellipsoid is observable and it evolves to a sphere as the annealing time increases until $t \sim$ 90s. At that time (approximately), the void shape achieves the final spherical shape as shown in Figure 5.

Irregularities on the output of the simulation could be observed due to a large mesh element size. Because of that fact, an approximation to an ellipsoid was performed to visualize the general trend and measure the different results.

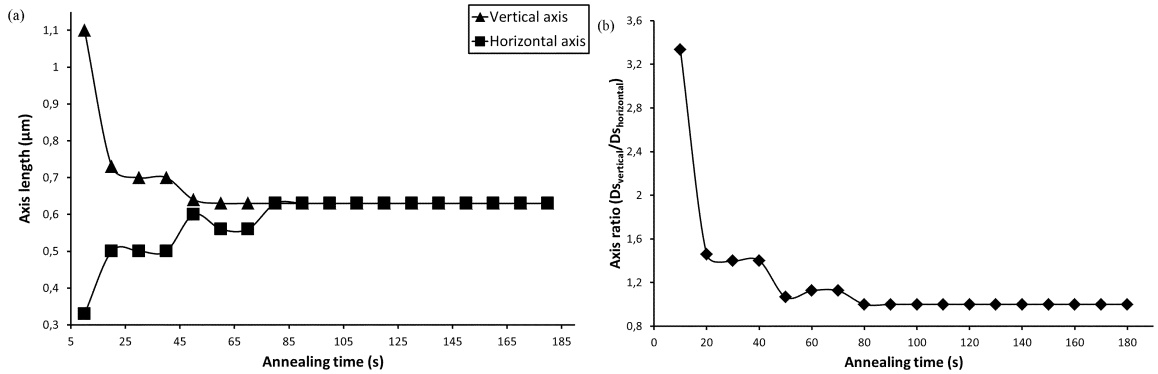

Fig. 6 Ellipsoid (a) and axis ratio (b) evolution with the annealing time of a trench with a trench diameter of 0.30 µm, trench length of 2 µm at 1100 °C.

The simulation of an initial cylindrical trench whose diameter is 0.30 μm and length is 2 μm with an annealing temperature of 1100 °C (Fig. 6) was performed. The results display a final spherical diameter of $d_{S,S}$ = 0.63 μm while the theoretical result, according to (2.24), would give $d_{S,T}$ = 0.56 μm. The relative error found was 12.5%, which is acceptable with respect to the simplifications made in the model.

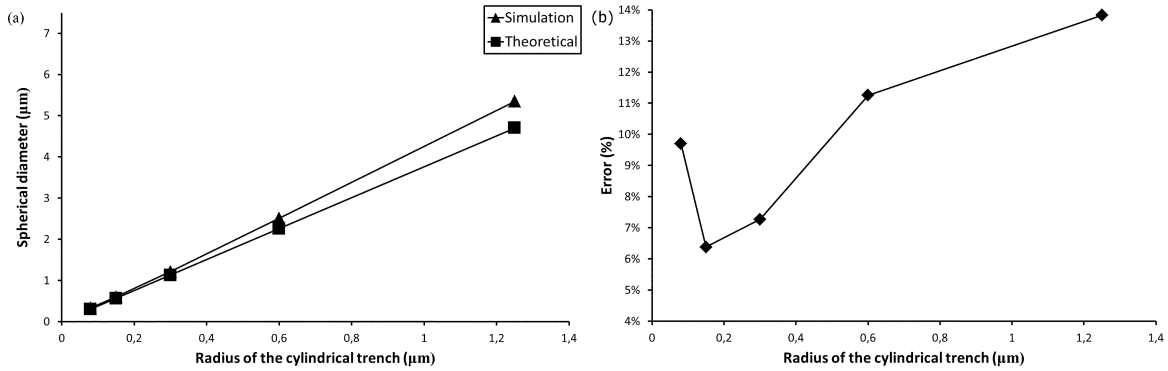

Fig. 7 Equilibrium spherical diameter depending on the cylindrical radius (a) and its relative error (b).

Different starting geometries of the trenches were also evaluated to observe the differences between the theoretically predicted geometries and the simulated ones. The temperature was fixed at 1100 ºC. The depths of the trench were varied using the following values: L_C = 0.1/0.5/1/2/3.5/5/7/10/15 μm. The different cylindrical radii are: R_C = 0.08/0.15/0.3/0.6/1.25 μm. The evaluation of the simulation results was taken from the circular shape obtained by the intersection of a horizontal cut-in plane in the middle of the formed spherical void shape (at equilibrium). That circular shape is the top-view of the corresponding spherical void. If more than one sphere were formed in the same column, only data from the deepest void shape was taken into account. After that, the average value of the acquired spherical diameters for each initial cylindrical radius was calculated and implemented.

Fig. 7 summarizes the evolution of different initial trenches, and compares them with the theoretical final equilibrium state using (2.24). It can be observed that the equilibrium spherical diameter grows linearly with the initial cylindrical radius. Furthermore, the higher the initial radius, the higher is the absolute error between the theoretical and simulated results. Regarding the relative error, it shows a variation of 6-14% along the results. The computed relative error seems to increase as the initial radius grows excepting for very small trenches where a higher than expected relative error is reached.

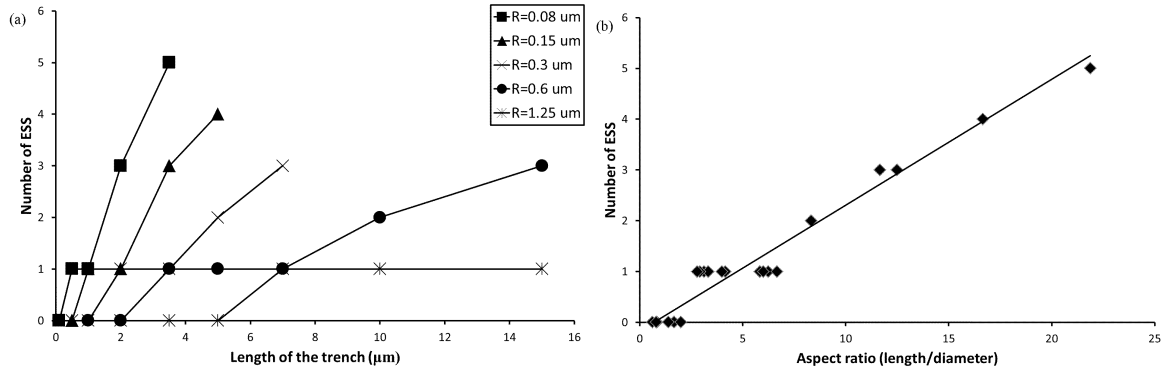

Fig. 8 Empty spaces in silicon (ESS) depending on the length of the trench (a) and on the aspect ratio (b).

Fig. 8 reflects the amount of created empty spaces in silicon with respect to the length of the trench at different cylindrical radius. The lower the cylindrical radius is, the more spheres are formed when increasing the length. The number of empty spaces of silicon is also dependent on the aspect ratio of the initial trench (length/diameter). The dependence, as illustrated in Fig. 8, can be approximated with a linear model.

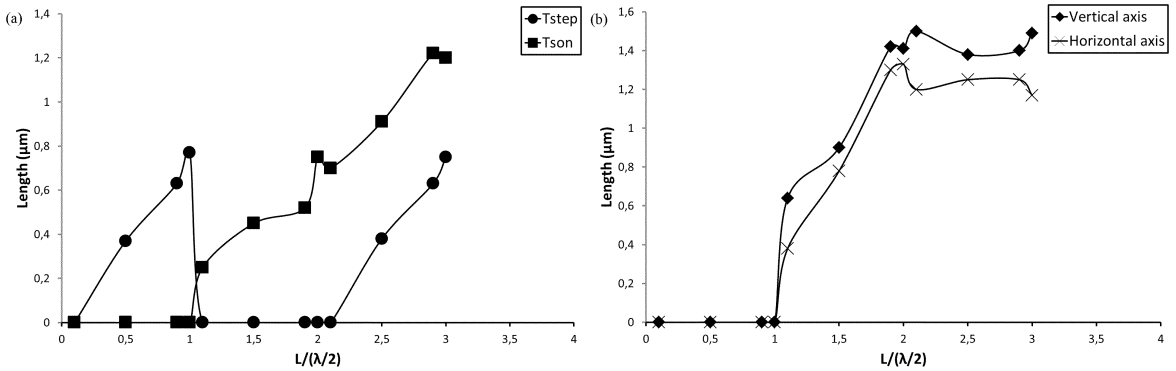

Fig. 9 Length impact on the step and SON layer (a) and the diameters of the ellipsoid formed at the bottom (b).

Further simulations were performed to study the dependence of the number of void shapes in silicon, after annealing, on the aspect ratio. A fixed cylindrical radius of 0.3 µm was used and a variation of the length of the trench from $0.1\lambda/2$ to 2λ µm was analyzed. Fig. 9a represents the size of the step (distance between the top surface and the silicon layer formed over the initial trench) and the size of the SON layer when changing the length of the initial cylindrical trench. Analyzing the results, it can be seen that the step size increases in the beginning until the trench closes (at $L_C > \lambda/2$). After that, there is no step until the full wavelength is reached ($L_C = \lambda$) and, from that point, it increases until it reaches the limit of the formation of a second empty space in silicon. Regarding the silicon on nothing layer (silicon layer formed over the empty space in silicon), it is created when a first empty space in silicon is formed. From that moment, silicon on nothing layer increases as the initial cylindrical depth grows.

Fig. 9b indicates how the shape of the empty space in silicon develops until reaching the equilibrium state with different trench depths. As it can be seen, the empty space in silicon increases in size with a deeper cylindrical trench. Once the full wavelength is reached ($L_C = \lambda$), the geometry does not significantly change. Note that the most perfect sphere (same horizontal and vertical axis size) is achieved when simulating a depth of the trench equal to the full wavelength. Consequently, it seems to be the most stable value in the model.

After those numerous simulations, it was possible to determine the number of empty spaces in silicon that are formed by the use of this simplified model, being n_S the integer number of empty spaces in silicon:

$$\begin{aligned} 0 < \frac{L_C}{2R_C} \le 2.22 &\Rightarrow n_S = 0 \\ \left[2.22 + 4.44(n_S - 1)\right] < \frac{L_C}{2R_C} \le \left(2.22 + 4.44 n_S\right) &\Rightarrow n_S \ge 1 \end{aligned} \tag{4.1}$$

Equation (4.1) gives an insight of the needed aspect ratio for getting one or more void shapes in silicon before performing the simulation or experiment. Therefore, it can be useful for predicting the final number of voids in a column beforehand. Comparing it with *Sato*'s work [13], an aspect ratio between 3 and 9.5 was concluded for one ESS. In this work, an aspect ratio between 2.22 and 6.66 for one ESS was obtained. While the lower limit is similar, the upper one is lower than Sato's experimental results. The differences can be derived from the source of the data and the simplifications done to this model. First of all, the source of the data obtained by *Sato et al.* and *Mizushima et al* is experimental [12], [13]. Their trenches are based on rectangular and squared base trenches while our characteristic theoretical values are based on a circular base. That should make a significant difference in addition to the several simplifications that were previously detailed.

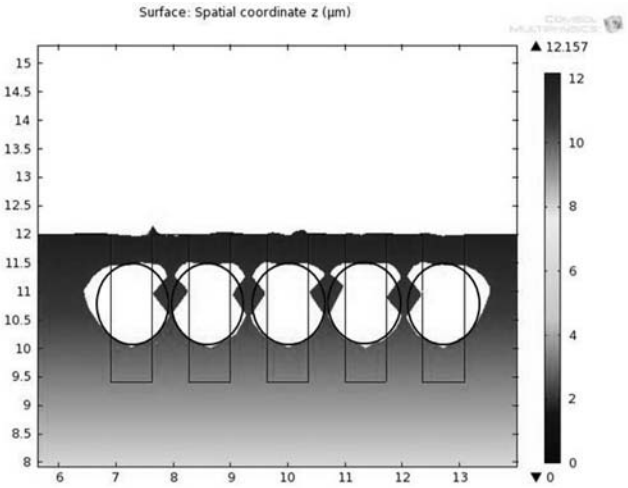

Fig. 10 Simulation of the structure defined on [15]. Black ellipses represent the measured geometry; the relative error is 6.62% and 2.63% for vertical and horizontal axis, respectively.

On the other hand, there exist further studies which partially agree with the critical values calculated in this work such as the critical aspect ratio of 7.2 in *Nichols*' work [34] for creating more than one ESS under the same cylindrical geometries. McLean [35], [36] observed the evolution of cylindrical liquid lead inclusions in an aluminium matrix under annealing. The critical aspect ratio for more than one ESS was 8. *Stapley and Beevers* [37], [38] studied the stability of sapphire whiskers in nickel whose effects were explained by the Ostwald ripening. They observed a spheroidization of the cylindrical structures between an aspect ratio of 3 and 6, quite close to our results. Finally, an experiment was carried out by *Sudoh et al.* [15] where the same cylindrical geometry was tested with an aspect ratio of 4. The result was one ESS as indicated in this work (Fig. 10).

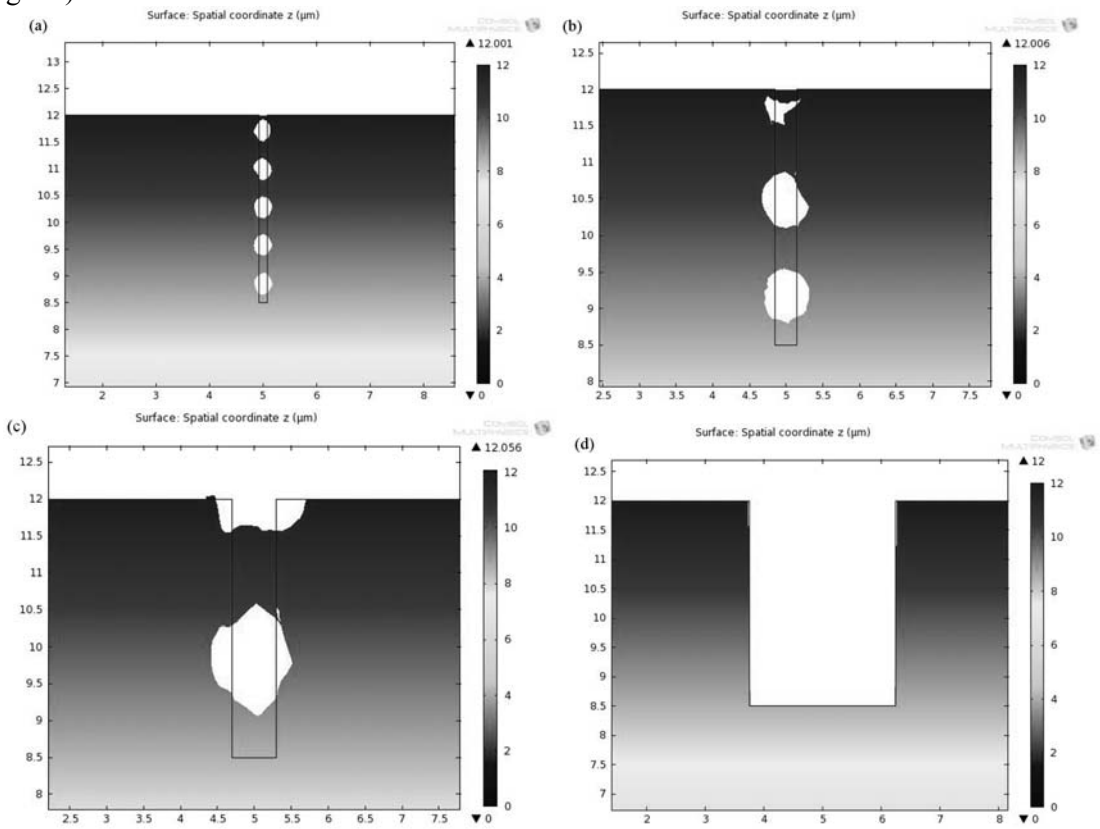

Fig. 11 Geometry evolution after an annealing time of 1000s at 1100 °C, *L*c = 3.5 μm and a cylindrical radius of 0.08 μm (a); 0.15 μm (b); 0.3 μm (c); 1.25 μm (d).

As the last point of this discussion, further simulations were performed using different cylindrical radii (other parameters are fixed) in order to see their effect. In Fig. 11, the increase of the cylindrical radius slows down the void shape evolution. As a consequence, the trench radius affects the void shape. Therefore, if the initial hole is too large, too much time is needed to make a full evolution (more distance), thus, one has to be aware of the available time for annealing when etching the initial trenches.

4.2 Temperature Dependence

The temperature dependence of the structure evolution is of significant importance because of its impact on the speed of the SON process. Using fixed geometrical parameters and annealing time, the state of the evolution of different temperatures is shown in Fig. 12.

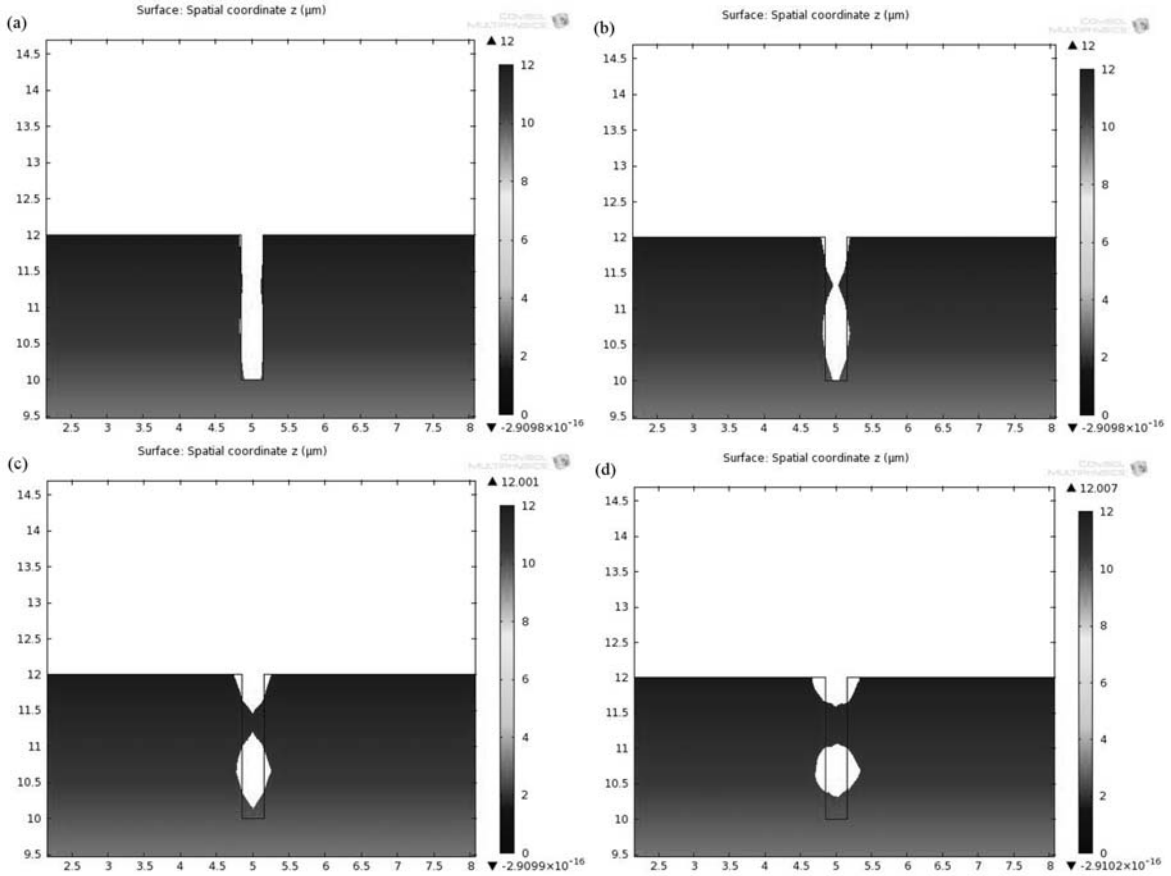

Fig. 12 Geometry evolution after an annealing time of 70 s, geometrical parameters: *L*c = 2 µm and cylindrical radius of 0.15 µm at: 900°C (a); 950°C (b); 1000°C(c); 1100°C (d).

The geometry obtained is an ellipsoid which gets more spherical with increasing temperature. At 1100 ºC, the evolution reaches the equilibrium state and further temperature increase does not change the geometry significantly as reflected in Fig. 12.

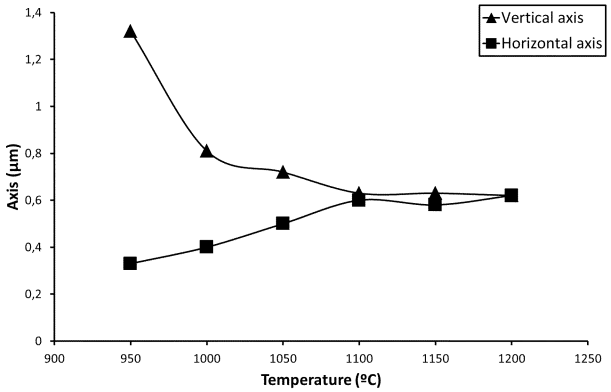

Fig. 13 Diameters obtained after an annealing time of 70 s at different temperatures.

Fig. 13 exhibits that the evolution is faster at higher temperatures until choosing a certain temperature from which the morphological change is so fast that it is not worth increasing it anymore. However, this limit depends on the initial geometry and annealing time.

5. Conclusions

The current research introduces a new way of computing the evolution of SON structures by the utilization of FEM and the algebraic Lagrangian-Eulerian (ALE) method through the software COMSOL Multiphysics®. The method proposed here relies on a succession of characteristic parameters obtained by deriving values from the theoretical evolution of a structure, in this case, from a cylindrical trench to a void sphere. Those characteristic parameters are employed to build a novel time-dependent and non-linear virtual curvature function, (3.9), which will drive the geometrical changes of the initial structure until it achieves the equilibrium. It simulates the effect of an initial perturbation that occurs at high temperatures and low pressures and it is implementable in other similar surface perturbation phenomena such as surface tension. The only mass transport phenomenon included for this kinetic analysis was surface diffusion which is a non-linear problem. The advantages of this method in COMSOL Multiphysics® are faster simulation times, possibility of computation with very coarse meshes (required for large displacements), improvements in the convergence and the simplification of the definition of the overall equation by the substitution of the scalar function (3.9) for a PDE (3.1).

Numerous simulations were performed with different initial radius, length, aspect ratio (length/diameter of the trench) and temperature. The results show a good agreement with the theory (6-14% of relative error) and they were compared to previous experimental and theoretical works, [12]-[13], [15], [34]-[38], which comprehend different materials and phenomena. The ones that used the same geometry as in this work and the surface diffusion as the main phenomenon, [15], [34], agreed on the presented results, especially, for aspect ratio dependence on the number of obtainable ESS.

Regarding the size of the step (distance between the top surface and the silicon layer formed in the trench) and the size of the SON layer when changing the length of the initial cylindrical trench, it can be seen that the step size increases in the beginning until the trench closes (at $L_C > \lambda/2$). After that, there is no step until the full wavelength is achieved ($L_C = \lambda$) and, from that point, it increases until it reaches the limit of the formation of a second empty space in silicon. Concerning the silicon on nothing layer (silicon layer formed over the empty space in silicon), it is created when a first empty space in silicon is formed. From that moment, silicon on nothing layer increases as the initial cylindrical depth grows.

Further observations indicate that the most perfect equilibrium sphere was formed at a trench length equal to the characteristic wavelength $\lambda_C = 8.89 R_C$ and that the temperature only increases or decreases the velocity of the evolution, being faster at higher temperatures. However, if the trench is large enough, no evolution is shown even at higher temperatures (Fig. 11).

Acknowledgements

The authors would like to thank the Saechsische Aufbaubank (SAB) and the Europaeischer SozialFonds (ESF) for the further financial support to the continuous development and improvement of this work by its awarded scholarship PhD program (number 100119076) for the national innovation in Saxony.

References

1. *Skotnicki T. and Monfray S.*, 'Silicon-On-Nothing (SON) Technology', *8th Int. Conf. on Solid-State and Integrated Circuit Technology Proc, Shangai,(2006) , 11 - 14.*
2. *Jurczak M., Skotnicki T., Paoli M., Tormen B., Martins J., Regolini J. L., Dutartre D., Ribot P., Lenoble D., Pantel R., Monfray S.,*'Silicon-on-Nothing (SON)-an Innovative Process for Advanced CMOS', *IEEE Trans. Electron Devices, **47** (2000), 2179 - 2187.*
3. *Monfray S., Skotnicki T., Morand Y., Descombes S., Paoli M., Ribot P., Talbot A., Dutartre C., Leverd F., Lefriec Y., Pantel R., Haond M., Renaud D., Nier M. E., Vizioz C., Louis D., Buffet N.,* 'SON (Silicon-On-Nothing) P-MOSFETs with totally silicided ($CoSi_2$) Polysilicon on 5nm-thick Si-films: The simplest way to integration of Metal Gates on thin FD channels', *Int. Electron Devices Meeting, (2001), 645 - 648.*
4. *Monfray S., Boeuf F., Coronel P., Bidal G., Denorme S., Skotnicki T.,* 'Silicon-On-Nothing (SON) applications for Low Power technologies', *Proc. of the 2008 IEEE Int. Conf. on Integrated Circuit Design and Technology, (2008), 1 - 4.*
5. *Villani P., Favilla S., Labate L., Novarini E., Ponza A.,Stella R.,* 'Evaluation of self-heating effects on an innovative SOI technology ("Venezia" process)', *Proc. of the 17th Int. Symp. on Power Semiconductor Devices & IC´s, (2005), 63 - 66.*
6. *Sugaya S., 'Semiconductor device with cavity and method of manufacture thereof'*, United States Patent US 7,253,479 B2*, 2007.*
7. *Sato T., Matsuo M., Mizushima Y., Tsunashima Y., Takagi S., 'Method for fabricating a localize SOI in bulk silicon substrate including changing first trenches formed in the substrate into unclosed empty space by applying heat treatment',* United States Patent US 7,507,634 B2, *2009.*
8. *Monfray S., Skotnicki T., Morand Y., Descombes S., Coronel P., Mazoyer P., Harrison S., Ribot P., Talbot A., Dutartre D., Haond M., Palla R., Le Friec Y., Leverd F., Nier M. E., Vizioz C., Louis D.,* '50nm – Gate All Around (GAA) – Silicon On Nothing (SON) – Devices: A Simple Way to Co-integration of GAAA Transistors within bulk MOSFET process', *Symp. on VLSI technology, (2002), 108 - 109.*
9. *Höllt L., Schulze J., Eisele I., Suligoj T., Jovanovic V., Thompson P. E.,* 'First sub-30nm vertical Silicon-On-Nothing MOSFET', *Proc. of the 31st Int. Convention on Information and Communication Technology, Electronics and Microelectronics MIPRO, (2008), 90 - 95.*
10. *Peng B., Yu T., Yu F.,* 'A Novel Process of Silicon-on-Nothing MOSFETs with Double Implantation', *Proc. of the 2007 IEEE Int. Conf. on Integration Technology, (2007), 237 - 240.*
11. *Bu W., Huang R., Li M., Yu T., Wang Y.,* 'A Novel Technique of Silicon-on-Nothing MOSFETs Fabrication by Hydrogen and Helium Co-implantation', *7th Int. Conf. on Solid-State and Integrated Circuits Technology, (2004), 269 - 272.*
12. *Mizushima I., Sato T., Taniguchi S., Tsunashimaj Y.,* 'Empty-space-in-silicon technique for fabricating a silicon-on-nothing structure', *Appl. Phys. Lett., 77 (2000)**,** 3290 - 3292.*
13. *Sato T., Mizushima I., Taniguchi S., Takenaka K., Shimonishi S., Hayashi H., Hatano M., Sugihara K., Tsunashima Y.,* 'Fabrication of Silicon-on-Nothing Structure by Substrate Engineering Using the Empty-Space-in-Silicon Formation Technique', *Jpn. J. Appl. Phys., **43** (2004), 12 - 18.*
14. *Sudoh K., Iwasaki H, Kuribayashi H., Hiruta R., Shimizu R.,* 'Numerical Study on Shape Transformation of Silicon Trenches by High-Temperature Hydrogen Annealing', *Jpn. J. Appl. Phys., **43** (2004), 5937 - 5941.*
15. *Sudoh K., Iwasaki H., Hiruta R., Kuribayashi H., Shimizu R.,* 'Void shape evolution and formation of silicon-on-nothing structures during hydrogen annealing of hole arrays on Si(001)', *J. Appl. Phys., **105** (2009), 083536-1 - 083536-5.*
16. *Mullins W. W., J. Appl. Phys,. **28** (1957), 333 - 339.*
17. *Steinhauser M. O., 'Computational Multiscale Modeling of Fluids and Solids Theory and Applications',* Springer, Berlin, 2008.
18. *S. Shin,* 'Computation of the curvature field in numerical simulation of multiphase flow', *J. Comput. Phys., **222** (2007), 872 - 878.*

19. *Engquist B., Tornberg A. K., Tsai R.,* 'Discretization of Dirac Delta Functions in Level Set Methods' *J. Comput. Phys.,* ***207*** *(2005), 28 – 51.*
20. *Yue P., Feng J. J., Liu C., Shen J.,* 'A diffuse-interface method for simulating two-phase flows of complex fluids', *J. Fluid Mech.,* ***515*** *(2004), 293 - 317.*
21. *Bruchon J., Munoz D. P., Valdivieso F., Drapier S., Pacquaut G,* '3D simulation of the matter transport by surface diffusion within a Level-Set context', *European Journal of Computational Mechanics,* ***19*** *(2010), 281 - 292*
22. *Burger M., Haußer F., Stöcker C., Voigt A.,* 'A level set approach to anisotropic flows with curvature regularization', *J. Comput. Phys.,* ***225*** *(1007), 183 - 205.*
23. *Smereka P.,* 'The Numerical Approximation of a Delta Function with Application to Level Set Methods', *Journal of Scientific Computing,* ***19*** *(2003), 439 - 460.*
24. *Lafaurie B., Nardone C., Scardovelli R., Zaleski S., Zanetti G.,* 'Modelling Merging and Fragmentation in Multiphase Flows with SURFER', *J. Comput. Phys.,* ***113*** *(1994), 134 - 147.*
25. *Olsson E., Kreis G.,* 'A conservative level set method for two phase flow', *J. Comput. Phys.,* ***210*** *(2005), 225 - 246.*
26. *Stein E., de Borst R., Hughes T. J. R., 'Encyclopedia of Computational Mechanics Volume 1: Fundamentals',* Wiley, Chichester, 2004.
27. *Suo Z.,* 'Motions of Microscopic Surfaces in Materials', *Adv. Appl. Mech.,* ***33*** *(1997),* ***193 - 294.***
28. *Mehrer H., ,Diffusion in Solids',* Springer, Berlin, 2007.
29. *Rayleigh L.,* 'On the instability of jets', *Proceedings of the London mathematical society,* ***10*** *(1878), 4 – 13.*
30. *Srolovitz D. J., Safran S. A.,* 'Capillary instabilities in thin films. I. Energetics' *J. Appl. Phys.,* ***60*** *(1986), 247 - 254.*
31. *Raessi M., Mostaghimi J., Bussmann M.,* 'Advecting normal vectors: A new method for calculating interface normal and curvatures when modeling two-phase flows', *J. Comput. Phys.,* ***226*** *(2007), 774 - 797.*
32. *Keeffe M. E., Umbach C. C., Blakely J. M.,* 'Surface self-diffusion on Si from the evolution of periodic atomic step arrays', *J. Phys. Chem. Solids,* ***55*** *(1994), 965 - 973.*
33. *Bermond J. M., Métois J. J., Egéa X., Floret F.,* 'The equilibrium shape of silicon', *Surf. Sci.,* ***330*** *(1995), 48 - 60.*
34. *Nichols F. A.,* 'On the spheroidization of rod-shaped particles of finite length', *J. Mater. Sci.,* ***11*** *(1976), 1077 - 1082.*
35. *McLean M.,* 'Kinetics of spheroidization of lead inclusions in aluminum', *Phil. Mag.,* ***27*** *(1973), 1253 - 1266.*
36. *McLean M., Loveday M. S.,* 'In-situ observations of the annealing of liquid lead inclusions entrained in an aluminium matrix', *J. Mater. Sci.,* ***9*** *(1974), 1104 - 1114.*
37. *Stapley A. J., Beevers C. J.,* 'The stability of sapphire whiskers in nickel at elevated temperatures. Part 1: General morphological and chemical stability', *J. Mater. Sci.,* ***8*** *(1973), 1287 - 1295.*
38. *Stapley A. J., Beevers C. J.,* 'The stability of sapphire whiskers in nickel at elevated temperatures. Part 2: The kinetics of morphological changes over the temperature range 1100 to 1400°C', *J. Mater. Sci.,* ***8*** *(1973), 1296 - 1306.*